

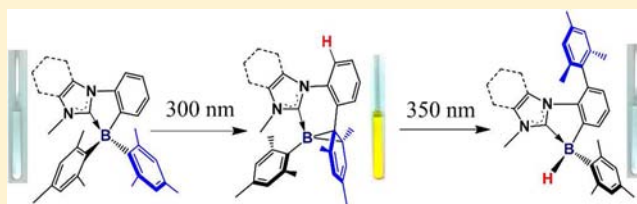
Stepwise Intramolecular Photoisomerization of NHC-Chelate Dimesitylboron Compounds with C–C Bond Formation and C–H Bond Insertion

Ying-Li Rao, Leanne D. Chen, Nicholas J. Mosey, and Suning Wang*

Department of Chemistry, Queen's University, Kingston, Ontario K7L 3N6, Canada

S Supporting Information

ABSTRACT: C,C-chelate dimesitylboron (BMes₂) compounds containing an N-heterocyclic carbene (NHC) donor have been obtained. Single-crystal X-ray diffraction analyses established that the boron atom in these compounds is bound by four carbon atoms in a distorted tetrahedral geometry. Compared to previously reported N,C-chelate dimesitylboron compounds, the new C,C-chelate boron compounds have a much larger HOMO–LUMO energy gap (>3.60 eV). They do, however, respond to UV irradiation (300 nm) in the same manner as N,C-chelate BMes₂ compounds do, undergoing photoisomerization and converting to an intensely colored (yellow or orange) isomer **A** quantitatively, with a high quantum efficiency (0.60–0.75). NMR and single-crystal X-ray diffraction analyses established that the structure of **A** is similar to the dark isomers obtained from N,C-chelate BMes₂ compounds. However, unlike the N,C-chelate dark isomers that have the tendency to thermally reverse back to the light colored isomers, the isomers **A** of the C,C-chelate BMes₂ are thermally stable and no reverse isomerization was observed even when heated to 80 °C (or 110 °C) for hours. The most unusual finding is that isomers **A** undergo further photoisomerization when irradiated at 350 nm, forming a new colorless species **B** nearly quantitatively. NMR and single-crystal X-ray diffraction analyses established the structure of isomer **B**, which may be considered as an intramolecular C–H insertion product via a borylene intermediate. Mechanistic aspects of this unusual two-step photoisomerization process have been examined by DFT computational studies.



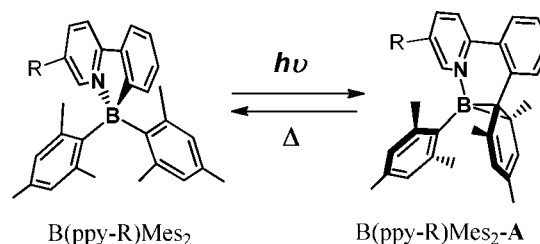
INTRODUCTION

N-heterocyclic carbenes (NHCs) are well-known for their ability to stabilize rare main group species¹ such as borylenes, boroles,² silylenes, disilylenes, disilynes,³ germynes,⁴ diboranes,⁵ P₂, P₄, As₂,⁶ and Ga₂,⁷ and so forth. Unusual and exciting chemical properties and reactivity have been frequently observed for NHC-stabilized main group compounds,^{1–7} which further drives the intense research interest and activities in NHC-main group chemistry. Nonetheless, much earlier research on main group NHC compounds has focused on monodentate NHC ligands. Main group compounds that contain chelate ligands involving NHC donors have hardly been explored, although NHC-containing chelate ligands involving a donor atom such as oxygen or nitrogen are well-known and have been extensively explored for transition metal chemistry.^{8,9}

We have been particularly interested in aryl-cyclometalating or C,C-chelate NHC ligands based on the consideration that these ligands contain two strongly σ -donating carbon atoms and should be capable of acting as a new type of chelate scaffolds for building new main-group π -conjugated materials. Many examples of transition metal complexes with aryl-cyclometalating NHC ligands have been reported previously and used successfully in catalysis and OLEDs.⁹ In contrast, main-group examples especially those with a boron as the central atom remain unexplored.¹⁰ Our other motivation in

investigating organoboron compounds that contain an NHC chelating ligand is to develop new photoresponsive organoboron compounds. We recently reported a new class of boron-based photochromic compounds based on B(ppy)Mes₂ (ppy = 2-phenylpyridine),¹¹ shown in Scheme 1.

Scheme 1. Photoisomerization of B(ppy-R)Mes₂



This class of compounds display a unique photoisomerization phenomenon, transforming from a colorless or light colored isomer to a dark colored isomer **A** quantitatively, upon irradiation by light (Scheme 1), with moderate to high quantum yields.¹¹ The N,C-chelate ligand plays a critical role in this unusual photoisomerization phenomenon. The steric

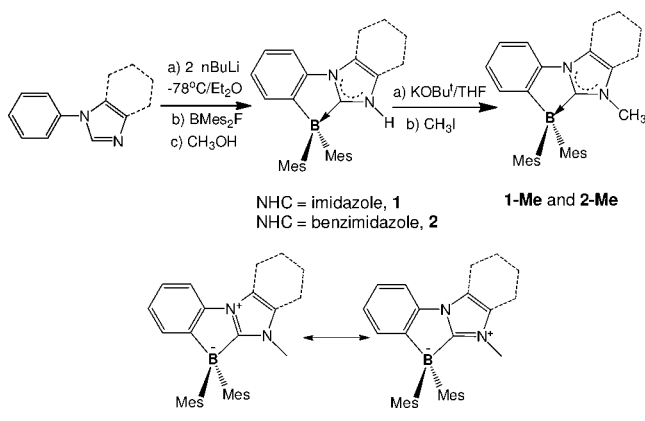
Received: May 7, 2012

Published: June 11, 2012

congestion imposed by the mesityl groups and the charge transfer transition from the mesityl to the N,C-chelate π^* orbital were found to be the key driving forces for the photoisomerization of the N,C-chelate BMe_2 compounds. The pyridyl moiety in $\text{B}(\text{ppy})\text{Me}_2$ and derivatives, albeit not affected by isomerization, plays a vital anchoring role, keeping the boron chromophore intact through the photoisomerization process. NHC ligands are much stronger σ donors than pyridyl. Thus, replacing the pyridyl with a NHC donor may allow us to achieve a new class of photoresponsive organoboron compounds and discover new photochemical reactivity of organoboron compounds.

With this in mind, we designed and synthesized two families of C,C-chelate BMe_2 compounds, namely, compounds **1** and **2**, and their methylated derivatives **1-Me** and **2-Me** (Scheme 2). We have found that **1-Me** and **2-Me** undergo unusual

Scheme 2. Synthetic Procedures and the Two Resonance Structures of 1, 2, 1-Me, and 2-Me



stepwise photoisomerization, generating two distinct isomers in the process. The details of our investigation on the new photoresponsive organoboron system are reported herein.

RESULTS AND DISCUSSION

Synthesis and Structures of 1, 2, 1-Me, and 2-Me. The syntheses of compounds **1** and **2** were accomplished by a straightforward one-pot procedure shown in Scheme 2. Double lithiation of *N*-phenyl imidazole or *N*-phenyl benzimidazole at -78°C in diethylether, followed by the addition of 1 equiv of BMe_2F yielded the lithium salt $\text{Li}[\text{B}(\text{C,C-chelate})\text{Me}_2]$. The possibility to double lithiate *N*-phenylimidazole was previously demonstrated by Canac and co-workers.¹² Addition of CH_3OH to the corresponding solution of the lithium salt generated compounds **1** and **2** in moderate yields (50% for **1** and 30% for **2**). **1** and **2** can be then converted quantitatively to the methylated derivatives **1-Me** and **2-Me** by the addition of a base (KO^tBu) and CH_3I . Compounds **1**, **2**, **1-Me**, and **2-Me** are colorless, air-stable, and can be purified by column chromatography. They are fully characterized by NMR, single-crystal X-ray diffraction, and elemental analyses. The two key resonance structures of these compounds are also shown in Scheme 2.

The crystal structures of **1-Me** and **2-Me** are shown in Figure 1. The structural diagrams of **1** and **2** can be found in the Supporting Information. As shown by Figure 1 and the key bond lengths and angles around the boron atom in Table 1, compounds **1**, **2**, **1-Me**, and **2-Me** have structural features similar to those of $\text{B}(\text{ppy})\text{Me}_2$ and derivatives.¹¹ For example,

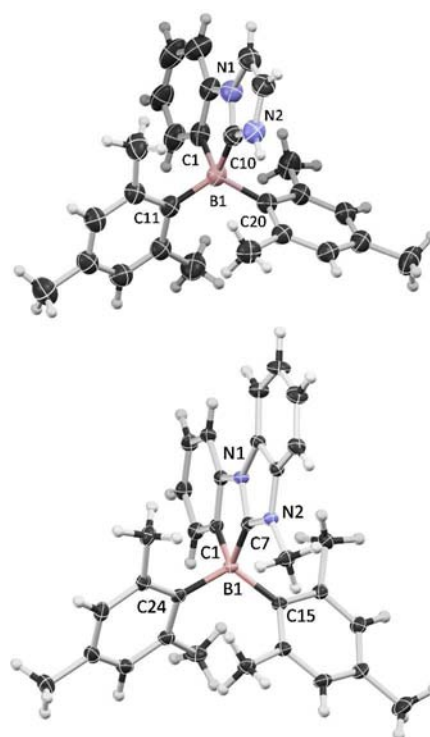


Figure 1. Crystal structures of **1-Me** (top) and **2-Me** (bottom) with 50% thermal ellipsoids and labeling schemes for key atoms.

Table 1. Important Bond Lengths (Å) and Angles (deg) of 1, 2, 1-Me, and 2-Me

compd.	B–C _{Ph}	B–C _{NHC}	B–C _{Mes}
1	1.650(7)	1.672(6)	1.657(6), 1.643(7)
1-Me	1.653(7)	1.644(7)	1.638(7), 1.646(7)
2	1.638(2)	1.653(2)	1.639(2), 1.666(2)
2-Me	1.663(2)	1.639(2)	1.651(2), 1.653(2)
compd.	C _{Ph} –B–C _{NHC}	C _{Mes} –B–C _{Mes}	
1	92.9(4)	117.5(4)	
1-Me	94.3(3)	115.1(4)	
2	94.3(2)	116.5(1)	
2-Me	94.2(1)	113.6(1)	

the B–C_{Ph} and B–C_{Mes} bond lengths are all considerably longer than the typical B–C bonds observed in noncongested four-coordinate boron compounds (e.g., $\text{B}(\text{ppy})\text{Ph}_2$)^{11c} but similar to those in sterically congested four-coordinate boron that contain a BMe_2 group.^{11,13} The B–C_{NHC} bond lengths are also all longer than previously reported typical B–C_{NHC} bond lengths in tetrahedral boron compounds.² One notable difference is that the B–C_{NHC} bond lengths in the non-methylated compounds **1** and **2** (1.672(6) and 1.653(2) Å) are longer than those in the methylated compounds **1-Me** and **2-Me** (1.644(7) and 1.639(2) Å), which may be attributed to the greater electron donating ability of methyl, compared to a H atom.

Electronic Properties of 1, 2, 1-Me, and 2-Me. Compared to N,C-chelate $\text{B}(\text{ppy})\text{Me}_2$, the new C,C-chelate compounds have a much larger HOMO–LUMO or optical energy gap and do not have any absorption in the visible region at all. Instead, they all have intense absorption bands in the UV region of 250–350 nm, as shown in Figure 2. The absorption maxima of **1** and **1-Me** are about 5–10 nm higher in energy

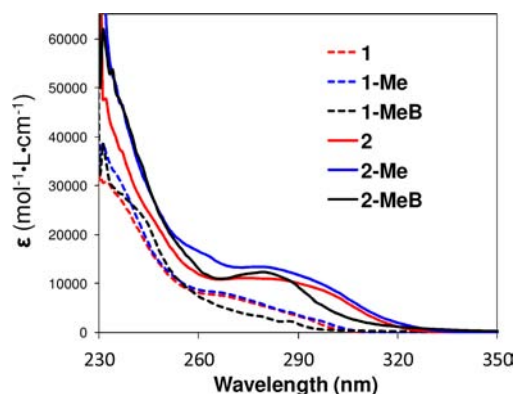


Figure 2. UV-vis absorption spectra of **1**, **1-Me**, **1-MeB**, **2**, **2-Me**, and **2-MeB** in CH_2Cl_2 ($\sim 1.0 \times 10^{-5}$ M).

than those of **2** and **2-Me**. The absorption edges (~ 320 nm) of **1** and **1-Me** are about 20–30 nm higher in energy than those (~ 345 nm) of **2** and **2-Me**, which can be attributed to the greater conjugation of the C,C-chelate ligand in **2** and **2-Me**.

Electrochemical data indicate that the narrowing of the HOMO–LUMO gap from **1-Me** to **2-Me** is mainly caused by the stabilization of the LUMO level (-1.94 to -2.14 eV), which is in agreement with the trend suggested by DFT calculation results (Figure 3, see Supporting Information for 2-

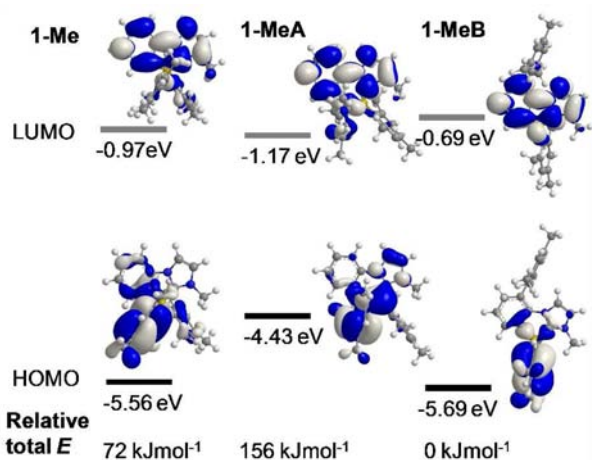


Figure 3. DFT calculated total energy, HOMO/LUMO energy, and diagrams of **1-Me**, **1-MeA**, and **1-MeB** (isocontour value = 0.02).

Me data). Furthermore, electrochemical data support that the large HOMO–LUMO gaps of **1-Me** and **2-Me**, compared to those of $\text{B}(\text{ppy})\text{Mes}_2$ (LUMO level = -2.50 eV, determined from CV data) are caused mainly by the high LUMO level of the C,C-chelate compounds. **2** and **2-Me** display weak purple-blue fluorescence at $\lambda_{\text{max}} = 410$ nm in toluene, which is also much higher in energy than that of $\text{B}(\text{ppy})\text{Mes}_2$ ($\lambda_{\text{max}} = 480$ nm). The fluorescence quantum efficiency was determined to be 0.11 for **2-Me**, and 0.10 for **2**. No appreciable fluorescence was observed for **1** and **1-Me**. Absorption spectral data and electrochemical data are summarized in Table 2.

TD-DFT computational results confirmed that the transition from the ground state to the first excited state of the C,C-chelate compounds is dominated by the HOMO to LUMO transition, which is a charge transfer from the mesityl to the π^* orbital of the C,C-chelate backbone as shown in Figure 3. The

Table 2. Absorption and Electrochemical Data

compd.	absorp. λ , nm, (log ϵ)	E^{red} (V) ^a	E^{ox} (V) ^a	optical gap (eV)	LUMO (eV)	HOMO (eV)
1	264 ^b (3.89)			4.06		
1-Me	265 ^b (3.92)	-2.32		3.87	-1.94 ^d	-5.81 ^f
1-MeA	426 ^c (3.50)	-2.30	-0.01	2.45	-1.80 ^f	-4.24 ^e
1-MeB	260 ^b (3.86)			4.18		
2	286 ^b (4.03)			3.78		
2-Me	290 ^b (4.06)	-2.06		3.65	-2.14 ^d	-5.79 ^f
2-MeA	456 ^c (4.06)	-2.00	0.13	2.30	-2.09 ^f	-4.38 ^e
2-MeB	280 ^b (4.05)			3.75		

^aRelative to Ag/AgCl reference electrode, recorded in DMF, $\text{FeCp}_2^{+/0} = 0.55$ V. ^b λ_{max} in CH_2Cl_2 . ^c λ_{max} in toluene. ^dFrom the reduction potential. ^eDetermined from the oxidation potential. ^fFrom the optical energy gap and the reduction potential or the oxidation potential.

HOMO–LUMO diagrams of **1-Me** and **2-Me** bear striking resemblance to those of $\text{B}(\text{ppy})\text{Mes}_2$. Thus, based on the similarity of molecular and electronic structures of **1-Me** and **2-Me** with those of $\text{B}(\text{ppy})\text{Mes}_2$, we anticipated that the new C,C-chelate BMes_2 compounds are very likely to undergo photoisomerization in the same manner as the N,C-chelate compounds.

Photoisomerization. 1-Me/2-Me to 1-MeA/2-MeA. To examine the response of the new C,C-chelate compounds toward light, we irradiated them using UV light at 300 nm, approximately the absorption maxima. The UV-vis spectral change was recorded in toluene. ¹H NMR spectral change was recorded in C_6D_6 . As shown in Figure 4, upon irradiation by

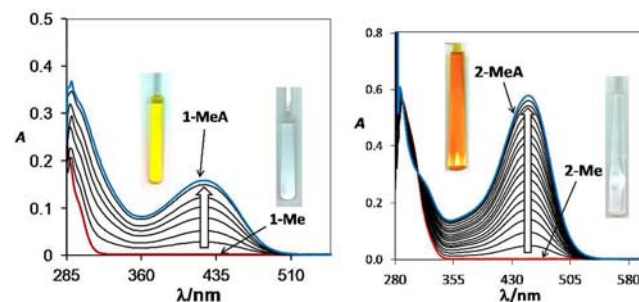


Figure 4. UV-vis spectra showing the conversion of **1-Me** (left) and **2-Me** (right) to **1-MeA** and **2-MeA**, respectively, in toluene irradiated at 300 nm, recorded with time intervals of a few seconds between each spectrum. Inset: photographs showing the color change of the samples before and after irradiation.

UV light, the C,C-chelate compounds undergo a distinct spectral change, with a new low energy absorption band appearing and growing with irradiation time, which can be attributed to the new isomer ($\lambda_{\text{max}} = 426$ nm for **1-MeA**, $\lambda_{\text{max}} = 456$ nm for **2-MeA**). This spectral change accounts for the change of the compounds from colorless to bright yellow (**1-Me**) or orange (**2-Me**).

¹H and ¹¹B NMR experiments showed that the methylated compounds **1-Me** and **2-Me** undergo clean and quantitative

isomerization upon irradiation at 300 nm, forming the new isomers **1-MeA** and **2-MeA**, respectively (see Supporting Information), while the response of **1** and **2** is complex with evident decomposition, which may be attributed to the acidic proton of the imidazolium. Thus, we focused our study on photoisomerization of **1-Me** and **2-Me**.

Unlike N,C-chelate compounds, where the C–C bond formation is restricted between a mesityl and the carbon donor atom of the chelate ligand, in the C,C-chelate compounds **1-Me** and **2-Me** because both donor atoms from the chelate ligand are carbon atoms, the C–C bond formation could occur at either the phenyl carbon site or the imidazolyl carbon site. As illustrated by the ^1H NMR spectra in Figure 5, the isomer **1-MeA** or **2-MeA** shows two characteristic olefinic proton peaks

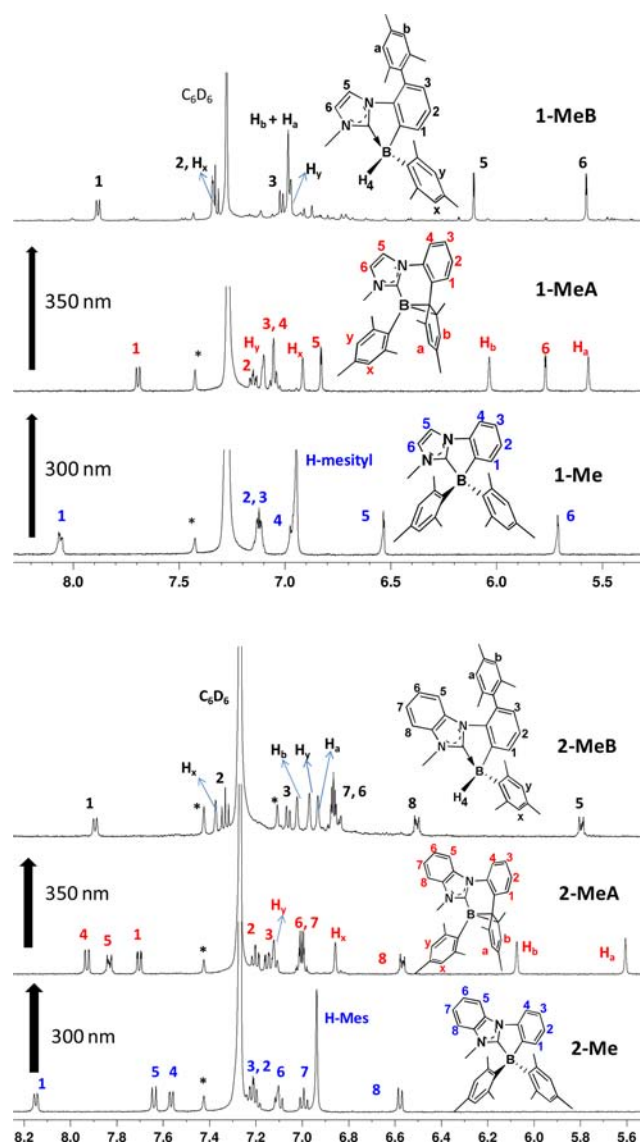


Figure 5. ^1H NMR spectral change (olefin and aromatic region) of **1-Me** (top)/**2-Me** (bottom) upon irradiation at 300 and 350 nm, respectively, showing their full conversion to **1-MeA**/**2-MeA**, and the subsequent conversion to **1-MeB**/**2-MeB**. The spectra were recorded in C_6D_6 at 25 °C. The aliphatic region of the same spectra can be found in the Supporting Information. The spin side bands are marked by asterisks (*). Additional time-lapsed NMR spectra showing the two-step isomerization can be found in Supporting Information.

that can be attributed to the H_a and H_b protons of the cyclohexadienyl group, similar to those observed for the $\text{B}(\text{ppy})\text{Mes}_2\text{-A}$ isomer shown in Scheme 1. Furthermore, the ^{11}B NMR spectral change (see Supporting Information) from -9.26 to -25.86 ppm for **1-Me**, and -8.98 to -19.70 ppm for **2-Me** follows the same trend as that observed for $\text{B}(\text{ppy})\text{Mes}_2$. Thus, the NMR data support that the yellow and orange isomers from **1-Me** and **2-Me** likely have similar structures as those of $\text{B}(\text{ppy})\text{Mes}_2\text{-A}$. To firmly establish the structures of **1-MeA** and **2-MeA**, 2D NMR experiments (COSY and NOESY, see Supporting Information) were performed for both compounds, which confirmed that they indeed have the structures shown in Figures 5.

Further evidence supporting the structures of **1-MeA** and **2-MeA** were obtained from the single-crystal X-ray diffraction analysis data of **2-MeA**. The crystal structure of **2-MeA** is shown in Figure 6. Its geometrical parameters are similar to

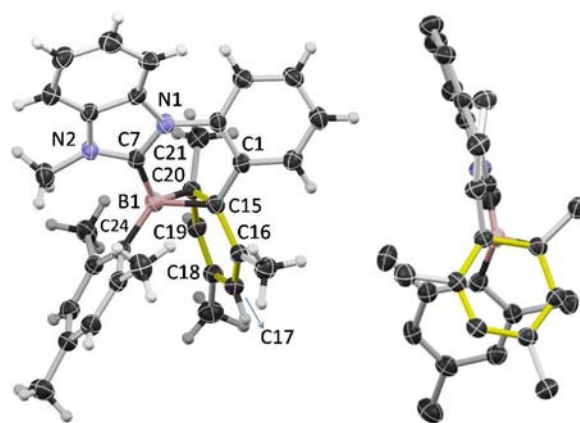


Figure 6. The crystal structure of **2-MeA** with 50% thermal ellipsoids and labeling schemes for key atoms (left) and the side view of the structure with H atoms omitted (right). Important bond lengths (Å) and angles (°): B(1)–C(7) 1.539(5), B(1)–C(15) 1.684(5), B(1)–C(20) 1.621(5), B(1)–C(24) 1.601(5), C(1)–C(15) 1.488(5), C(15)–C(20) 1.548(5), C(15)–C(16) 1.484(4), C(16)–C(17) 1.346(5), C(17)–C(18) 1.443(5), C(18)–C(19) 1.355(4), C(19)–C(20) 1.466(5); C(7)–B(1)–C(24) 117.3(3), C(15)–B(1)–C(20) 55.8(2), B(1)–C(15)–C(20) 60.2(2), B(1)–C(20)–C(15) 64.2(2).

those of the dark isomer of a N,C-chelate compound, $\text{BMes}_2(\text{Py-N-Ph-IN})\text{-A}$ (Py-N-Ph-IN = 1-Phenyl-2-(2-Pyridyl)-indolyl), the only other dark isomer crystal structure we reported recently.^{11e} The B(1)–C(7) bond (1.539(5) Å) in **2-MeA** is much shorter than that of **2-Me**. The C(15)–C(20) bond (1.548(5) Å) is typical of a C–C single bond while the bond lengths (1.346(5), 1.355(4) Å) of C(16)–C(17) and C(18)–C(19) agree well with typical C=C bonds, thus, confirming that the transformed mesityl group can indeed be described as a cyclohexadienyl. The structural features of the BC_2 -cyclohexadienyl moiety in **2-MeA** are also similar to a BC_2 -naphthyl moiety in boron-carbene compounds reported by Braunschweig and co-workers.^{2b} The C,C-chelate benzene ring and the benzimidazolyl ring are twisted out of coplanarity with a dihedral angle of 19.4°, attributable to the interactions of the two *ortho*-H atoms. The NMR data and the crystal structure of **2-MeA** confirmed that the C–C bond coupling occurs exclusively at the phenyl site of the C–C chelate. This finding indicates that the NHC-carbon donor atom in these molecules

play an anchoring role, in the same manner as the pyridyl does in $B(\text{ppy})\text{Mes}_2$.

The photoisomerization of **1-Me/2-Me** to **1-MeA/2-MeA** is very efficient and the quantum efficiency has been determined in toluene using ferrioxalate actinometry at 297 nm excitation.¹⁴ For **1-Me** to **1-MeA**, the quantum efficiency was found to be ~ 0.75 , similar to that of $B(\text{ppy})\text{Mes}_2$ (~ 0.80), while for **2-Me** to **2-MeA**, the efficiency is lower, ~ 0.60 . These data support that the C,C-chelate $B\text{Mes}_2$ compounds undergo very efficient photoisomerization.

Despite the structural similarity of **1-MeA** and **2-MeA** with the dark isomers of N,C-chelate $B\text{Mes}_2$ compounds, **1-MeA** and **2-MeA** have a much greater stability toward oxygen in solution and the solid state, compared to the N,C-chelate analogues. In fact, the orange crystals of **2-MeA** are stable under air for days.

Electrochemical analysis data (CV) show that **1-MeA** and **2-MeA** have a distinct low oxidation potential (-0.55 and -0.41 V, vs $\text{FeCp}_2^{+/0}$) similar to that^{11c} of the dark blue isomer $B(\text{ppy})\text{Mes}_2\text{-A}$ (Figure 7 and Table 2). The greater stability of

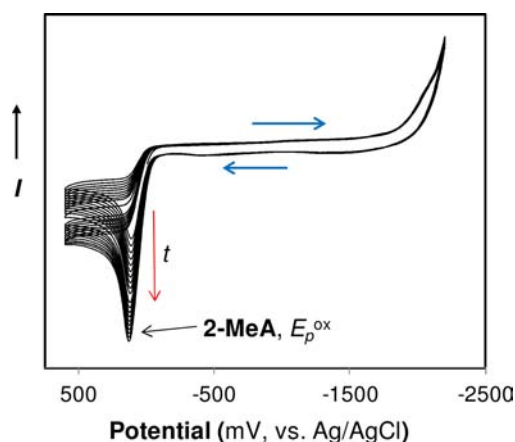
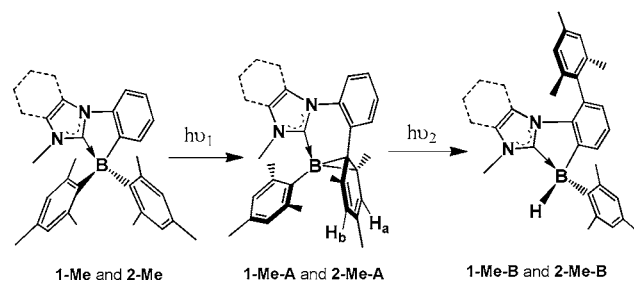


Figure 7. CV diagrams showing the appearance and the growth of the oxidation peak of **2-MeA** with time (t) when the DMF solution of **2-Me** is irradiated at 300 nm with a hand-held UV lamp, with NBu_4PF_6 as the electrolyte, and a scan rate of 150 mV s^{-1} . $E_{1/2}(\text{FeCp}_2^{+/0}) = 0.55 \text{ V}$.

1-MeA and **2-MeA** toward oxygen, compared to the N,C-chelate analogues is therefore quite surprising. On the basis of UV-vis and CV data, the HOMO level of **1-MeA** and **2-MeA** is more than 1 eV above that of **1-Me** and **2-Me** while the LUMO level experiences little change (see Table 2). The color difference between the yellow **1-MeA**/orange **2-MeA** and the dark blue $B(\text{ppy})\text{Mes}_2\text{-A}$ is therefore caused mainly by the relatively high LUMO level (~ -2.0 eV) of **1-MeA** and **2-MeA**, compared to that of $B(\text{ppy})\text{Mes}_2\text{-A}$ (~ -2.50 eV), leading to a higher $S_0 \rightarrow S_1$ transition energy for the C,C-chelate compounds. This trend is in good agreement with the DFT computational results shown in Figure 3. The electron density distribution in **1-MeA** and **2-MeA** was found to be similar to that of $B(\text{ppy})\text{Mes}_2\text{-A}$ with the HOMO level being dominated by contributions from the BC_2 triangular ring (Figure 3). The computational results also show that **1-MeA** and **2-MeA** are about 70–80 kJ less stable than **1-Me** and **2-Me**. This energy difference is much less than that between $B(\text{ppy})\text{Mes}_2$ and $B(\text{ppy})\text{Mes}_2\text{-A}$ (~ 115 kJ). Thus, the carbene donors appear to exert a greater stabilization effect to the isomers **A**, compared to the pyridyl.

1-MeA/2-MeA to **1-MeB/2-MeB**. In sharp contrast to the behavior of $B(\text{ppy})\text{Mes}_2\text{-A}$ and its derivative compounds that can thermally reverse back to the more stable colorless or light colored isomers,¹¹ **1-MeA** and **2-MeA** have been found to have a very high thermal stability. The ^1H NMR spectra of **1-MeA** and **2-MeA** show no change at all after being heated at either 110°C in d_8 -toluene or 80°C in C_6D_6 for hours (see Supporting Information). However, remarkably, we observed that both **1-MeA** and **2-MeA** can be sensitized by light. When irradiated at 350 nm, **1-MeA** and **2-MeA** gradually lose their color, converting to a new colorless isomer **1-MeB** and **2-MeB**, respectively (Scheme 3). This process can be monitored by

Scheme 3. Stepwise Photoisomerization of **1-Me** and **2-Me**



UV-vis spectra (see Supporting Information), ^{11}B and ^1H NMR spectra. NMR spectra show that **1-MeA** and **2-MeA** transform cleanly to **1-MeB** and **2-MeB** (Figure 5 and Supporting Information), respectively, although this photoisomerization step is much less efficient, compared to the isomerization of **1-Me/2-Me** to **1-MeA/2-MeA**. Full conversion can only be achieved after the samples were irradiated at 350 nm for a few days at the typical NMR concentration scale (~ 1 mg sample in 0.5 mL of solvent), while under the same conditions, using 300 nm excitation, the full conversion of **1-Me/2-Me** to **1-MeA/2-MeA** can be achieved in less than 30 min. Interestingly, the conversion of **1-MeA** and **2-MeA** to **1-MeB** and **2-MeB** is considerably less efficient and slower, when irradiated at their absorption maxima (420 and 450 nm, respectively), compared to excitation at 350 nm, under the same conditions.

1-MeB and **2-MeB** are air-stable and colorless. The structures of **1-MeB** and **2-MeB** were first established by ^1H , ^{11}B , COSY and NOESY NMR spectra. In the $^1\text{H}\{^{11}\text{B}\text{-decoupled}\}$ NMR spectra of both **1-MeB** and **2-MeB**, a peak at 4.23 and 4.35 ppm, respectively, was observed, which can be assigned to a B–H proton. In the $^{11}\text{B}\{^1\text{H}\text{-coupled}\}$ NMR spectra, **1-MeB** and **2-MeB** display a distinct doublet at -19.4 and -19.3 ppm, respectively, with a coupling constant of 85 Hz, characteristic of $^1J_{\text{B-H}}$ coupling^{2b,c,e,15,16} (see Supporting Information). The 6 methyl groups on the two mesityls are all resolved with 6 distinct chemical shifts in the ^1H NMR spectra of **1-MeB** and **2-MeB**, due to the asymmetric environment around the B atom. The absorption spectra of **1-MeB** and **2-MeB** resemble those of **1-Me** and **2-Me** (Figure 2), with the $S_0 \rightarrow S_1$ transition being a charge transfer from a mesityl to the chelate (Figure 3), shown by DFT computational results.

The crystal structure of **1-MeB** was determined by single-crystal X-ray diffraction analysis, which fully corroborates the structural features established by NMR experiments. As shown in Figure 8, the C,C-chelate remains bound to the B atom in **1-MeB**. In addition, the B atom is bound to one mesityl group and one H atom (located directly from a difference Fourier

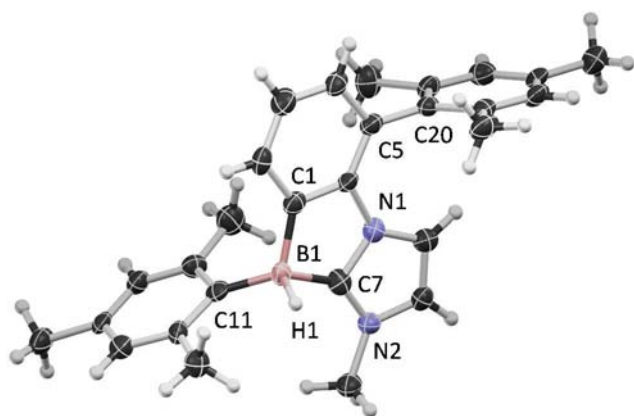
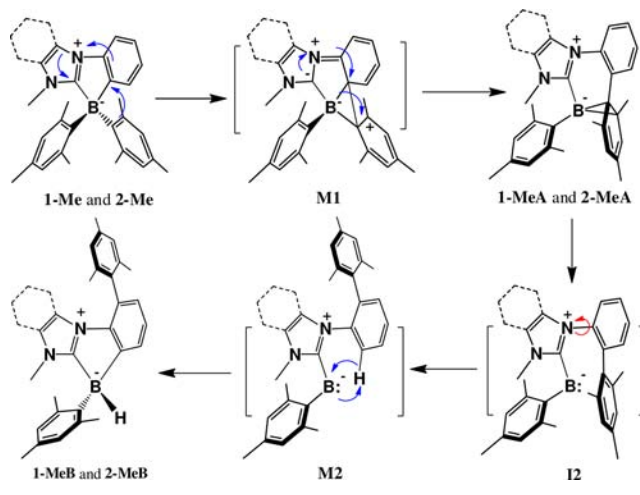


Figure 8. Crystal structure of **1-MeB** with 50% thermal ellipsoids and labeling schemes for key atoms. Important bond lengths (Å) and angles (°): B(1)–C(1) 1.621(11), B(1)–C(7) 1.618(11), B(1)–C(11) 1.609(11), B(1)–H(1) 1.20(5); C(1)–B(1)–C(7) 95.3(6), C(11)–B(1)–H(1) 113(2), C(1)–B(1)–C(11) 117.5(7), C(7)–B(1)–C(11) 117.5(7).

map) in a distorted tetrahedral geometry. The B(1)–H(1) bond length was determined to be 1.20(5) Å, in agreement with typical terminal B–H bond lengths reported previously.^{2b,c,e,15,16} The second mesityl group forms a C–C bond with a carbon atom of the phenyl ring with a typical bond length (C(5)–C(20) = 1.488(10) Å). Compared to those of **1-Me** and **2-Me**, the B–C bonds in **1-Me-B** are considerably shorter, which can be attributed to the reduced steric congestion around the B center.

Mechanism. Mechanistically, the photoisomerization of the C,C-chelate compound **1-Me/2-Me** to **1-MeA/2-MeA** likely follows a similar pathway as that of B(ppy)Mes₂ via a transition state **M1**, as shown in Scheme 4. Therefore, we will first

Scheme 4. Proposed Mechanism for the Stepwise Transformation of **1-Me** and **2-Me**



comment on the B(ppy)Mes₂ system. Our computational study on B(ppy)Mes₂ indicated that its transformation to the dark blue isomer B(ppy)Mes₂-A is not accessible on the ground state due to a very large activation energy. However, at the first excited state, [B(ppy)Mes₂]* is less stable than [B(ppy)Mes₂-A]*, thus, B(ppy)Mes₂ can readily transform to the dark isomer B(ppy)Mes₂-A, via the excited state.¹⁷ Because of the large

energy difference between B(ppy)Mes₂ and B(ppy)Mes₂-A, the activation barrier (determined experimentally to be ~110 kJmol⁻¹) for the reverse transformation of B(ppy)Mes₂-A to B(ppy)Mes₂ is thermally accessible.

Our attempts to map out the transition states and calculate the activation barrier for the thermal transformation of **1-Me** to **1-MeA** using DFT methods were unsuccessful. Nonetheless, we have identified an intermediate (**I1**) that is similar to that involved in the transformation of B(ppy)Mes₂, but at a much higher energy (~204 kJmol⁻¹ higher than **1-Me**, and 130 kJmol⁻¹ than **1-MeA**), as shown in Figure 9. This suggests that

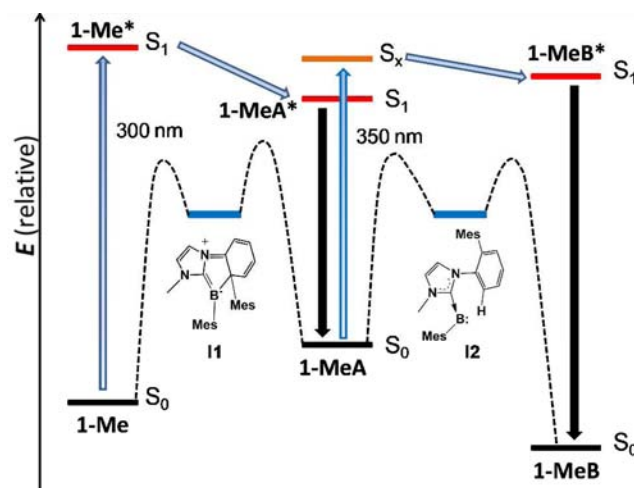


Figure 9. Energy diagrams showing the relative energies of **1-Me**, **1-MeA**, and **1-MeB** at the ground state (S_0) and at the first excited state (S_1). The arrows indicate the transformation pathways between the three isomers. The structures and relative energy levels of two intermediates at the ground state identified by DFT calculations are also shown. Peaks in the dashed curves connecting the structures represent estimated positions of transition states separating those structures.

the thermal activation barriers for both forward and reverse transformation of **1-Me** are much higher than those of B(ppy)Mes₂ and as a result, **1-Me** and **1-MeA** cannot interconvert thermally. Preliminary computational results on the first excited state indicates that [1-Me]* to [1-MeA]* transformation is a downhill process with an energy difference ~50 kJmol⁻¹, thus, the transformation of **1-Me** to **1-MeA** can occur readily via the excited state.

A computational study of the isomerization **1-MeA** to **1-MeB** was also performed. At the ground state, a highly energetic “borylene”-like intermediate **I2** was identified (~140 kJmol⁻¹ above **1-MeA**). The transition state connecting **1-MeA** and **I2** could not be located; however, the energy of the transition state must be at least as high as that of **I2**, suggesting a large activation energy for the transformation from **1-MeA** to **1-MeB**, rendering that process inaccessible via a thermal pathway. The formation of **I2** may be described as a cheletropic boron elimination¹⁸ from **1-MeA**.

At the first excited state, [1-MeB]* is less stable than [1-MeA]* by ~30 kJmol⁻¹. Thus, in order to convert **1-MeA** to **1-MeB** via the excited state, **1-MeA** needs to be excited above the first excited state. This provides a plausible explanation as to why a 350 nm excitation energy is required to achieve reasonable conversion of **1-MeA/2-MeA** to **1-MeB/2-MeB** and the fact that the second photoisomerization step is much less

efficient than the first step. It is very likely that a “borylene”-like species **I2** is involved in the excited state transformation of isomer **A** to **B**. A simple rotation around the N–C bond in **I2** would bring the *ortho*-H atom of the benzene ring close to the boron center (**M2**), activating the C–H bond (Scheme 4). The possible involvement of a borylene species in intramolecular C–H insertion reactions was proposed in several previously reported organoboron systems, where the proposed “borylene” species was generated *in situ* via chemical reduction of a borane, followed by C–H insertion.^{1e,2c,16} It is conceivable that in our system, the C,C-chelate ligand stabilizes the “borylene” intermediate **I2** generated in the excited state, leading to C–H bond activation and the isolation of compounds **1-MeB** and **2-MeB**. The selective activation of an aryl C–H bond over an aliphatic C–H bond (e.g., the methyl group in the mesityl) may be facilitated by the involvement of the π^* orbital of the benzene ring in stabilizing the transition state and the greater stability of the resulting 5-membered ring in **1-MeB** (versus the 6-membered ring in methyl activation).

On the basis of the calculated data, among the three isomers, **1-MeB** is the most stable isomer, 75 kJmol⁻¹ below **1-Me** and 145 kJmol⁻¹ below **1-MeA**. Thus, the transformation of **1-MeA** to **1-MeB** is highly favored thermodynamically. Schematically, the photoisomerization pathways based on experimental observations and DFT computational results are shown in Figure 9.

CONCLUSIONS

We have shown that C,C-chelate BMe₂ compounds that contain one NHC-donor atom have structures and electronic properties similar to those of N,C-chelate BMe₂ compounds, and as a result, this class of compounds undergo highly efficient and clean photoisomerization in the same manner as the N,C-chelate BMe₂ compounds do. There are, however, several distinct differences between the N,C-BMe₂ and C,C-BMe₂ compounds. First of all, the carbene donor greatly stabilizes the dark isomers of the C,C-chelate compounds, such that they are much more stable toward air than the corresponding N,C-chelate compounds, and cannot thermally reverse back to the colorless isomers. Second, the dark isomers of the C,C-chelate compounds can undergo further photoisomerization, producing a new isomer that involves intramolecular C–H bond activation. The same phenomenon has not been observed at all in any of the N,C-chelate BMe₂ compounds we investigated previously. The robustness of the C,C-chelate BMe₂ compounds toward photolysis and their ability to undergo clean and stepwise photoisomerization are truly remarkable, opening many new research opportunities in accessing unusual structures/species/reactivity via the excited state.

EXPERIMENTAL SECTION

General Procedure. Diethyl ether was used directly from Pure Solv Solvent Purification System (Innovative Technology, Inc., Amesbury, MA). All starting materials were purchased from Aldrich Chemicals Co. All reactions were carried out under nitrogen atmosphere, using Schlenk and vacuum line techniques. The ¹H, ¹³C, ¹¹B, and 2D HH COSY, NOESY NMR spectra were recorded on Bruker Avance 500 MHz spectrometer. UV–vis spectra were recorded on a Cary50 UV–visible spectrometer. Fluorescence spectra were recorded on a Photon Technologies International Quanta Master model C-60 spectrometer. High-resolution mass spectra (HRMS) were obtained from an Applied Biosystems Qstar XL spectrometer. Elemental analyses were conducted at Laboratoire d'Analyse Élémentaire de l'Université de Montréal.

Fluorescence quantum yield of compound **2-Me** was measured in dilute degassed toluene solution (Abs. = ~0.1) at room temperature using the relative quantum yield method using 9,10-diphenylanthracene as the reference standard ($\Phi = 0.90$).¹⁹

Computational Studies. DFT and TD-DFT calculations were performed at the CAM-B3LYP/SVP level of theory.²⁰ Test calculations demonstrated that this level of theory accurately reproduced the experimentally determined UV–vis spectrum of a reference compound in the same class as those considered here. All reactant, product and intermediate structures were optimized without constraints, and characterized as minima on the potential energy surface through frequency calculations. Excited state energies were determined through TD-DFT calculations.

The stationary points were optimized a second time at the B3LYP/6-311++G** level of theory²¹ in order to generate the orbital eigenvalues of the HOMO and LUMO given in Figure 3. This was done to be consistent with previous computational work on similar compounds. All calculations were performed with the Gaussian 09 Software.²²

Syntheses of 1 and 1-Me. *n*-Butyllithium (2.5 M, 1.7 mL, 4.2 mmol) was slowly added to a solution of 1-phenylimidazole (0.3 g, 2.1 mmol) in Et₂O (100 mL) at –78 °C. The solution was warmed to room temperature and stirred for 3 h. A diethyl ether solution of BMe₂F (0.62 g, 2.1 mmol) was then added dropwise at –78 °C. The resulting solution was slowly warmed to room temperature and stirred overnight. After the addition of excess methanol, the solution was then concentrated under vacuum. Purification by chromatography on silica gel (hexane/CH₂Cl₂) yielded compound **1** as a white solid, which was recrystallized from hexane/CH₂Cl₂ (0.40 g, 50%). ¹H NMR (CDCl₃, 25 °C, ppm): 9.02 (s), 7.67 (d, 1H, *J* = 7.0 Hz), 7.38 (d, 1H, *J* = 1.5 Hz), 7.15–7.31 (m, 3H), 7.87 (d, 1H, *J* = 1.5 Hz), 6.70 (s, 4H), 2.23 (s, 6H), 1.88 (s, 12H). ¹³C NMR (CDCl₃, 25 °C, ppm): 140.2, 140.2, 134.7, 133.1, 129.0, 126.7, 124.9, 120.0, 111.6, 110.3, 77.3, 77.0, 76.8, 24.9, 20.7. ¹¹B NMR (CDCl₃, 25 °C, ppm): –9.66 (s). ¹¹B NMR (CDCl₃, 160 MHz, 25 °C, ppm): –9.57 (s). Anal. Calcd for C₂₇H₃₀BN₂: C, 82.44; H, 7.69; N, 7.12. Found: C, 82.58; H, 7.49; N, 7.09.

Compound **1** (100 mg, 0.25 mmol) and KO^tBu (40 mg, 0.35 mmol) were dissolved in 5 mL of THF in a vial; excess CH₃I (0.5 mL) was then added to the solution. The resulting solution was stirred overnight at room temperature, with white precipitate generated during the progress of the reaction. After filtration of the KI salt and concentration of the filtrate under vacuum, **1-Me** was obtained almost quantitatively, which was recrystallized from hexane/CH₂Cl₂. ¹H NMR (CD₂Cl₂, 25 °C, ppm): 7.60 (d, 1H, *J* = 7.5 Hz), 7.52 (d, 1H, *J* = 1.5 Hz), 7.33 (d, 1H, *J* = 7.5 Hz), 7.18 (td, 1H, ³*J* = 7.5 Hz, ⁴*J* = 1.5 Hz), 7.09 (td, 1H, ³*J* = 7.5 Hz, ⁴*J* = 1.5 Hz), 7.00 (d, 1H, *J* = 1.5 Hz), 6.66 (s, 4H), 3.57 (s, 6H), 2.20 (s, 6H), 1.83 (s, 12H). ¹³C NMR (CD₂Cl₂, 25 °C, ppm): 140.4, 140.1, 132.8, 132.6, 129.1, 126.1, 125.3, 124.5, 111.5, 110.8, 35.2, 24.7, 20.4. The carbene carbon could not be observed in ¹³C NMR spectra. In 2D ¹H–¹³C HMBC spectra, the cross peak between the carbene carbon and the protons from *N*-methyl showed up at 174.5 ppm. ¹¹B NMR (CD₂Cl₂, 160 MHz, 25 °C, ppm): –9.75 (s). Anal. Calcd for C₂₈H₃₁BN₂·0.17CH₂Cl₂: C, 80.45; H, 7.51; N, 6.66. Found: C, 80.39; H, 7.79; N, 6.65. The presence of CH₂Cl₂ (~0.5 per molecule) in the crystal lattice was confirmed by X-ray crystallographic analysis.

Syntheses of 2 and 2-Me. The ligand 1-phenyl-benzimidazole was synthesized according to a literature procedure.²³ Compound **2** was synthesized and purified in the same manner as described for compound **1**, and recrystallized from hexane/CH₂Cl₂ (30% yield) as a colorless solid. ¹H NMR (CD₂Cl₂, 25 °C, ppm): 9.69 (s), 8.15 (d, 1H, *J* = 10.8 Hz), 7.84 (d, 1H, *J* = 8.4 Hz), 7.58–7.66 (m, 3H), 7.49 (t, 1H, *J* = 10 Hz), 7.37 (t, 1H, *J* = 10 Hz), 7.23 (t, 1H, *J* = 10 Hz), 6.87 (s, 4H), 2.21 (s, 6H), 1.92 (s, 12H). ¹³C NMR (CD₂Cl₂, 25 °C, ppm): 141.7, 140.1, 134.9, 134.1, 133.2, 129.0, 128.2, 125.9, 124.8, 113.2, 112.8, 112.1, 25.2, 20.4. ¹¹B NMR (CD₂Cl₂, 160 MHz, 25 °C, ppm): –9.65 (s). HRMS (TOF MS EI⁺): Calcd, 442.2580; Observed, 442.2591.

Compound **2-Me** was obtained almost quantitatively in the same way as **1-Me**, and recrystallized from hexane/CH₂Cl₂. ¹H NMR (CD₂Cl₂, 25 °C, ppm): 8.20 (d, 1H, *J* = 7.5 Hz), 7.81 (d, 1H, *J* = 8.0 Hz), 7.68 (d, 1H, *J* = 7.5 Hz), 7.61 (td, 1H, ³*J* = 6.0 Hz, ⁴*J* = 2.0 Hz), 7.56–7.60 (m, 2H), 7.30 (t, 1H, *J* = 7.5 Hz), 7.13 (t, 1H, *J* = 7.0 Hz), 6.69 (s, 4H), 3.57 (s, 6H), 2.21 (s, 6H), 1.88 (s, 12H). ¹³C NMR (CD₂Cl₂, 25 °C, ppm): 140.3, 140.7, 137.2, 133.1, 132.3, 129.2, 128.0, 125.8, 124.9, 124.4, 112.9, 112.4, 111.5, 31.3, 24.9, 20.4. The carbene carbon could not be observed in ¹³C NMR spectra. In 2D ¹H–¹³C HMBG spectra, the cross peak between the carbene carbon and the protons from N-methyl showed up at 183.1 ppm. ¹¹B NMR (C₆D₆, 160 MHz 25 °C, ppm): –8.98 (s). Anal. Calcd for C₃₃H₃₃BN₂: C, 84.21; H, 7.29; N, 6.14. Found: C, 83.85; H, 7.31; N, 6.18.

Photoisomerization of 1-Me and 2-Me and Syntheses of 1-MeA, 1-MeB, 2-MeA, and 2-MeB. General Procedures. Photoisomerization experiments were carried out in toluene or benzene under nitrogen using a Rayonet Reactor RPR-100. The progress of the photoisomerization was monitored by ¹H NMR spectra.

The photoisomerization quantum efficiencies of **1-Me** to **1-MeA** and **2-Me** to **2-MeA** at 297 nm were determined using ferrioxalate actinometry.¹⁴ An Ocean Optics fiber optic spectrophotometer connected to a four-way temperature-controlled cuvette holder from Quantum Northwest via 400 μm optical fibers was used to measure the absorbance. The irradiation source was a 200 W Hg/Xe lamp attached to a monochromator (Photon Technology International).

1-Me to 1-MeA. Compound **1-MeA** was obtained quantitatively via irradiation of **1-Me** at 300 nm under nitrogen. The photoisomerization quantum efficiency was determined to be ~0.75. On a typical NMR concentration scale (e.g., 1 mg of compound in ~0.5 mL of C₆D₆), this conversion is completed in less than 0.5 h. Compound **1-MeA** can be crystallized readily from toluene/hexanes as a yellow crystalline solid. ¹H NMR (25 °C, 500 MHz, ppm, C₆D₆): 7.69 (d, 1H, *J* = 10 Hz), 7.15 (td, 1H, *J* = 10 Hz, *J* = 2.5 Hz), 7.10 (s, 1H), 7.06 (m, 2H), 6.92 (s, 1H), 6.84 (d, 1H, *J* = 2.5 Hz), 6.03 (s, 1H), 5.78 (d, 1H, *J* = 2.5 Hz), 5.64 (s, 1H), 3.01 (s, 3H), 2.73 (s, 3H), 2.33 (s, 3H), 2.23 (s, 3H), 2.07 (s, 3H), 1.97 (s, 3H), 0.85 (s, 3H). ¹¹B NMR (25 °C, 160 MHz, C₆D₆): –25.9 ppm.

1-MeA to 1-MeB. Compound **1-MeB** was obtained nearly quantitatively via continuous irradiation of **1-MeA** at 350 nm under nitrogen. The photoisomerization quantum efficiency is ~0.001. **1-MeB** can be isolated as a colorless crystalline solid from a C₆D₆/hexanes solution. Because the conversion of **1-MeA** to **1-MeB** is very slow and inefficient (taking a few days to reach completion for a solution of ~1 mg of **1-MeA** in 0.5 mL of solvent), bulk conversion was not performed. ¹H NMR (25 °C, 500 MHz, ppm, C₆D₆): 7.87 (d, 1H, *J* = 7.5 Hz), 7.32 (t, 1H, *J* = 7.5 Hz), 7.33 (s, 1H), 7.01 (d, 1H, *J* = 7.5 Hz), 6.98 (s, 2H), 6.97 (s, 1H), 6.10 (d, 1H, *J* = 2.0 Hz), 5.58 (d, 1H, *J* = 2.0 Hz), 3.26 (s, 3H), 2.63 (s, 3H), 2.46 (s, 3H), 2.37 (s, 3H), 2.32 (s, 3H), 2.11 (s, 3H), 1.73 (s, 3H). The B–H peak was observed in a ¹H {¹¹B decoupled} NMR spectrum: 4.23 (s, 1H). ¹¹B NMR (25 °C, 160 MHz, C₆D₆): –19.4, ppm, ¹*J*_{B–H} = 85 Hz. HRMS (TOF MS EI⁺): calcd, 406.2580; observed, 406.2591.

2-Me to 2-MeA. Compound **2-MeA** was obtained quantitatively via irradiation of **2-Me** at 300 nm under nitrogen. The photoisomerization quantum efficiency is ~0.60. Compound **2-MeA** can be crystallized readily from toluene/hexanes as a orange crystalline solid. **2-MeA** ¹H NMR (25 °C, 500 MHz, ppm, C₆D₆): 7.92 (dd, 1H, *J* = 10 Hz, *J* = 1.0 Hz), 7.83 (m, 1H), 7.70 (dd, 1H, *J* = 7.5 Hz, *J* = 1.5 Hz), 7.20 (td, 1H, *J* = 7.0 Hz, *J* = 1.5 Hz), 7.15 (td, 1H, *J* = 8.0 Hz, *J* = 1.5 Hz), 7.12 (s, 1H), 7.00 (m, 2H), 6.86 (s, 1H), 6.57 (m, 1H), 6.08 (s, 1H), 5.61 (s, 1H), 3.04 (s, 3H), 2.97 (s, 3H), 2.33 (s, 3H), 2.26 (s, 3H), 1.95 (s, 3H), 1.94 (s, 3H), 0.95 (s, 3H). ^a The coupling constant was not obtained due to the complexity induced by second order coupling.

¹¹B NMR (25 °C, 160 MHz, C₆D₆): –24.5 ppm.

2-MeA to 2-MeB. Compound **2-MeB** was obtained nearly quantitatively via continuous irradiation of **2-MeA** at 350 nm under nitrogen. The photoisomerization is very inefficient (Q.E. = ~0.001). As a result, bulk conversion was not performed. Compound **2-MeB** can be isolated as a colorless crystalline solid. ¹H NMR (25 °C, 500 MHz, ppm, C₆D₆): 7.89 (d, 1H, *J* = 7.5 Hz), 7.37 (s, 1H), 7.33 (t, 1H,

J = 7.5 Hz), 7.06 (d, *J* = 7.5 Hz), 7.02 (s, 1H), 6.97 (s, 1H), 6.93 (s, 1H), 6.85 (m, 2H), 6.51 (m, 1H), 5.58 (m, 1H), 3.30 (s, 3H), 2.96 (s, 3H), 2.48 (s, 3H), 2.39 (s, 3H), 2.21 (s, 3H), 2.06 (s, 3H), 1.78 (s, 3H). The B–H peak was observed in a ¹H {¹¹B decoupled} NMR spectrum: 4.35 (s, 1H). (^aThe coupling constant was not obtained due to the complexity induced by second order coupling.)

¹¹B NMR (25 °C, 160 MHz, C₆D₆): –19.7 ppm, doublet, ¹*J*_{B–H} = 85 Hz. HRMS (TOF MS EI⁺): calcd, 456.2737; observed, 456.2749.

X-ray Crystallographic Analysis. Single crystals of compounds **1**, **2**, **1-Me**, and **2-Me** were obtained from the solution of CH₂Cl₂/toluene/hexanes while single-crystals of **1-MeB** and **2-MeA** were obtained from toluene/hexanes solutions at 298 K. Data were collected on a Bruker AXS Apex II single-crystal X-ray diffractometer with graphite-monochromated Mo K α radiation, operating at 50 kV and 30 mA at 180 K. Data were processed on a PC with the aid of the Bruker SHELXTL software package (version 6.14)²⁴ and corrected for absorption effects. All structures were solved by direct methods. The crystal lattice of **1-Me** contains disordered solvent molecules which are most likely CH₂Cl₂ (~0.5 per molecule of **1-Me**). To improve the quality of the structural refinements, solvent contributions were removed by the Squeeze routine of Platon program.²⁵ The crystals of **1-MeB** are very small and diffract weakly, resulting in a low ratio of observed reflections versus parameters, despite the 60 s/frame exposure time employed for data collection. Nonetheless, we were able to fully refine the structure of **1-MeB**. The hydrogen atom bound to the boron atom in **1-MeB** was located directly from a difference Fourier map and refined successfully. All non-hydrogen atoms were refined anisotropically. The positions of hydrogen atoms other than the one bound to boron were calculated, and their contributions in structural factor calculations were included. The details of crystallographic data can be found in the Supporting Information. Crystal data for all structures have been deposited to the Cambridge Crystal Data Center (CCDC 877955–877960).

■ ASSOCIATED CONTENT

☛ Supporting Information

1D and 2D NMR data, photoisomerization data (UV–vis and NMR), computational data, electrochemical analysis data and diagrams, crystal structural data. This material is available free of charge via the Internet at <http://pubs.acs.org>.

■ AUTHOR INFORMATION

Corresponding Author

Wangs@chem.queensu.ca.

Notes

The authors declare no competing financial interest.

■ ACKNOWLEDGMENTS

We thank the Natural Sciences and Engineering Research Council of Canada for financial support, the High Performance Computing Virtual Laboratory (HPCVL) and WestGrid High Performance Computing consortium for computing facilities. We are in debt to Professor Victor Snieckus for his insights and suggestions on the isomerization mechanism shown in Scheme 4.

■ REFERENCES

- (1) (a) Bourissou, D.; Guerret, O.; Gabbai, F. P.; Bertrand, G. *Chem. Rev.* **2000**, *100*, 39. (b) Martin, D.; Melaimi, M.; Soleilhavou, M.; Bertrand, G. *Organometallics* **2011**, *30*, 5304. (c) Curran, D. P.; Solov'yev, A.; Brahmī, M. M.; Fensterbank, L.; Malacria, M.; Lacôte, E. *Angew. Chem., Int. Ed.* **2011**, *50*, 10294. (d) Wang, Y.; Robinson, G. H. *Dalton Trans.* **2012**, *41*, 337. (e) Wang, Y.; Robinson, G. H. *Inorg. Chem.* **2011**, *50*, 12326. (f) Wang, Y.; Robinson, G. H. *Chem. Commun.* **2009**, 5201. (g) Matsumoto, T.; Gabbai, F. P. *Organo-*

- metallics* **2009**, *28*, 4252. (h) Kronig, S.; Theuergarten, E.; Daniliuc, C. G.; Jones, P. G.; Tamm, M. *Angew. Chem., Int. Ed.* **2012**, *51*, 3240.
- (2) (a) Kinjo, R.; Donnadiou, B.; Celik, M. A.; Frenking, G.; Bertrand, G. *Science* **2011**, *333*, 610. (b) Bissinger, P.; Braunschweig, H.; Kraft, K.; Kupfer, T. *Angew. Chem., Int. Ed.* **2011**, *50*, 4704. (c) Bissinger, P.; Braunschweig, H.; Damme, A.; Dewhurst, R. D.; Kupfer, T.; Radacki, K.; Wagner, K. *J. Am. Chem. Soc.* **2011**, *133*, 19044. (d) Braunschweig, H.; Kupfer, T. *Chem. Commun.* **2011**, *47*, 10903. (e) Braunschweig, H.; Chiu, C.-W.; Kupfer, T.; Radacki, K. *Inorg. Chem.* **2011**, *50*, 4247.
- (3) (a) Wang, Y.; Xie, Y.; Wei, P.; King, R. B.; Schaefer, H. F.; Schleyer, P.; Robinson, G. H. *Science* **2008**, *321*, 1069. (b) Yamaguchi, T.; Sekiguchi, A.; Driess, M. *J. Am. Chem. Soc.* **2010**, *132*, 14061. (c) Tanaka, H.; Ichinohe, M.; Sekiguchi, A. *J. Am. Chem. Soc.* **2012**, *134*, 5540.
- (4) (a) Rupa, P. A.; Jennings, M. C.; Ragogna, P. J.; Baines, K. M. *Organometallics* **2007**, *26*, 4109. (b) Sidiropoulos, A.; Jones, C.; Stasch, A.; Klein, S.; Frenking, G. *Angew. Chem., Int. Ed.* **2009**, *48*, 9701.
- (5) (a) Grigsby, W. J.; Power, P. P. *Chem.—Eur. J.* **1997**, *3*, 368. (b) Moezzi, A.; Olmstead, M. M.; Power, P. P. *J. Am. Chem. Soc.* **1992**, *114*, 2715. (c) Wang, Y.; Quillian, B.; Wei, P.; Wannere, C. S.; Xie, Y.; King, R. B.; Schaefer, H. F.; Schleyer, P. v. R.; Robinson, G. H. *J. Am. Chem. Soc.* **2007**, *129*, 12412. (d) Wang, Y.; Quillian, B.; Wei, P.; Xie, Y.; Wannere, C. S.; King, R. B.; Schaefer, H. F.; Schleyer, P. v. R.; Robinson, G. H. *J. Am. Chem. Soc.* **2008**, *130*, 3298.
- (6) (a) Masuda, J. D.; Schoeller, W. W.; Donnadiou, B.; Bertrand, G. *J. Am. Chem. Soc.* **2007**, *129*, 14180. (b) Wang, Y.; Xie, Y.; Wei, P.; King, R. B.; Schaefer, H. F.; Schleyer, P. v. R.; Robinson, G. H. *J. Am. Chem. Soc.* **2008**, *130*, 14970. (c) Abraham, M. Y.; Wang, Y.; Xie, Y.; Wei, P.; Schaefer, H. F.; Schleyer, P. v. R.; Robinson, G. H. *Chem.—Eur. J.* **2010**, *16*, 432. (d) Wang, Y.; Xie, Y.; Abraham, M. Y.; Wei, P.; Schaefer, H. F.; Schleyer, P. v. R.; Robinson, G. H. *Chem. Commun.* **2011**, *47*, 9224.
- (7) Quillian, B.; Wei, P.; Wannere, C. S.; Schleyer, P. v. R.; Robinson, G. H. *J. Am. Chem. Soc.* **2009**, *131*, 3168.
- (8) (a) Kühn, O. *Chem. Soc. Rev.* **2007**, *36*, 592 and references therein. (b) Stephen, T.; Liddle, I.; Edworthy, S.; Arnold, P. L. *Chem. Soc. Rev.* **2007**, *36*, 1732 and references therein.
- (9) (a) Hitchcock, P. B.; Lappert, M. F.; Pye, P. L.; Thomas, S. J. *Chem. Soc., Dalton Trans.* **1979**, 1929. (b) Rubio, R. J.; Andavan, G. T. S.; Bauer, E. B.; Hollis, T. K.; Cho, J.; Tham, F. S.; Donnadiou, B. *J. Organomet. Chem.* **2005**, *690*, 5353. (c) Chang, C.-F.; Cheng, Y.-M.; Chi, Y.; Chiu, Y.-C.; Lin, C.-C.; Lee, G.-H.; Chou, P.-T.; Chen, C.-C.; Chang, C.-H.; Wu, C.-C. *Angew. Chem., Int. Ed.* **2008**, *47*, 4542. (d) Haneder, S.; Como, E. D.; Feldmann, J.; Rothmann, M. M.; Strohhriegel, P.; Lennartz, C.; Molt, O.; Münster, I.; Schildknecht, C.; Wagenblast, G. *Adv. Funct. Mater.* **2009**, *19*, 2416. (e) Chi, Y.; Chou, P.-T. *Chem. Soc. Rev.* **2010**, *39*, 638 and references therein. (f) Unger, Y.; Meyer, D.; Molt, O.; Schildknecht, C.; Münster, I.; Wagenblast, G.; Strassner, T. *Angew. Chem., Int. Ed.* **2010**, *49*, 10214.
- (10) After the submission of this manuscript, we learned that S. Yamaguchi and co-workers have synthesized and investigated related N-thienyl-benzimidazole C,C-chelate BMes₂ compounds, see: Nagura, K.; Saito, S.; Fröhlich, R.; Glorius, F.; Yamaguchi, S. *Angew. Chem., Int. Ed.* **2012**, *51*, DOI: 10.1002/anie.201204050.
- (11) (a) Rao, Y. L.; Amarne, H.; Zhao, S. B.; McCormick, T. M.; Martić, S.; Sun, Y.; Wang, R. Y.; Wang, S. *J. Am. Chem. Soc.* **2008**, *130*, 12898. (b) Baik, C.; Hudson, Z. M.; Amarne, H.; Wang, S. *J. Am. Chem. Soc.* **2009**, *131*, 14549. (c) Amarne, H.; Baik, C.; Murphy, S. K.; Wang, S. *Chem.—Eur. J.* **2010**, *16*, 4750. (d) Murphy, S. K.; Baik, C.; Lu, J. S.; Wang, S. *Org. Lett.* **2010**, *12*, 5266. (e) Amarne, H.; Baik, C.; Wang, R.; Wang, S. *Organometallics* **2011**, *30*, 665. (f) Baik, C.; Murphy, S. K.; Wang, S. *Angew. Chem., Int. Ed.* **2010**, *49*, 8224.
- (12) Canac, Y.; Duhayon, C.; Chauvin, R. *Angew. Chem., Int. Ed.* **2007**, *46*, 6313.
- (13) (a) Wakamiya, A.; Taniguchi, T.; Yamaguchi, S. *Angew. Chem., Int. Ed.* **2006**, *45*, 3170. (b) Fukazawa, A.; Yamaguchi, E.; Ito, E.; Yamada, H.; Wang, J.; Irle, S.; Yamaguchi, S. *Organometallics* **2011**, *30*, 3870. (c) Fukazawa, A.; Yamada, H.; Yamaguchi, S. *Angew. Chem., Int. Ed.* **2008**, *47*, 5582.
- (14) Montalti, M.; Credi, A.; Prodi, L.; Gandolfi, M. T. *Handbook of Photochemistry*, 3rd ed.; CRC/Taylor & Francis: Boca Raton, FL, 2006.
- (15) Allen, F. H.; Bruno, I. J. *Acta Crystallogr.* **2010**, *B66*, 380 and references therein.
- (16) (a) Curran, D. P.; Boussonnière, A.; Geib, S. J.; Lacôte, E. *Angew. Chem., Int. Ed.* **2012**, *51*, 1602. (b) Celik, M. A.; Sure, R.; Klein, S.; Kinjo, R.; Bertrand, G.; Frenking, G. *Chem.—Eur. J.* **2012**, *18*, 5676.
- (17) Chen, L. D.; Wang, S.; Mosey, N. J., unpublished work.
- (18) Anslyn, E. V.; Dougherty, D. A. *Modern Physical Organic Chemistry*; University Science Books: Sausalito, CA, 2006. (b) IUPAC. *Compendium of Chemical Terminology*, 2nd ed., McNaught, A. D., Wilkinson, A., Eds.; Blackwell Scientific Publications: Oxford, 1997.
- (19) (a) Demas, N. J.; Crosby, G. A. *J. Am. Chem. Soc.* **1970**, *92*, 7262. (b) Fery-Forgues, S.; Lavabre, D. *J. Chem. Educ.* **1999**, *9*, 1260.
- (20) (a) Yanai, T.; Tew, D.; Handy, N. *Chem. Phys. Lett.* **2004**, *393*, 51. (b) Schaefer, A.; Horn, H.; Ahlrichs, R. *J. Chem. Phys.* **1992**, *97*, 2571.
- (21) Becke, A. D. *J. Chem. Phys.* **1993**, *98*, 5648.
- (22) Frisch, M. J. et al.; *Gaussian 09*, Revision C.01; Gaussian, Inc.: Wallingford, CT, 2010.
- (23) Verma, A. K.; Singh, J.; Sankar, V. K.; Chaudhary, R.; Chandra, R. *Tetrahedron* **2007**, *48*, 4207.
- (24) *SHELXTL*, Version 6.14; Bruker AXS, 2000–2003.
- (25) (a) Spek, A. L. *Acta Crystallogr.* **1990**, *A46*, C34. (b) Spek, A. L. *PLATON—a Multipurpose Crystallographic Tool*; Utrecht University: Utrecht, The Netherlands, 2006.